Dynamic-Characteristics Analysis of an Independent Microgrid by a SOFC Triple Combined Cycle

Shin'ya Obara

Kitami Institute of Technology, Power Engineering Lab., Dep. of Electrical and Electronic Engineering

Koen-cho 165, Kitami, Hokkaido 090-8507, Japan

obara@mail.kitami-it.ac.jp

phone/FAX +81-157-26-9262

Abstract

The fuel cell triple combined cycle (SOFC-TCC) of rated power 1.4 MW consists of a solid oxide fuel cell (SOFC, 542 kW), a gas turbine (G/T, 550 kW), and a steam turbine (S/T, 308 kW). The relation of the frequency deviation based on the supply-and-demand difference of an independent microgrid which interconnects SOFC-TCC described in the top and large-scale photovoltaics was investigated by numerical analysis (MATLAB/Simulink R 2013a). As a result, because the following to load fluctuations of SOFC and S/T required 1.8 to 2 hours, being controlled to mainly correspond by governor free control of G/T about the load fluctuation for 2 hours or less was found. Furthermore, a microgrid with photovoltaics is strongly influenced in the magnitude of the inertia force of the G/T and S/T, the inertia system confirmed giving change to the power characteristics (frequency) from cyclic fluctuation (change for several minutes or less) to sustained fluctuation (change exceeding 20 minutes). From the analysis results, supply-

and-demand fluctuations of long times, such as daily or seasonally, etc. is mainly controlled by output adjustment of the SOFC and S/T, the operation controlled by setting of the governor free control of the G/T and the inertia system of rotary machines is appropriate for the power fluctuation of a cycle shorter than the fluctuation cycle described in the top.

Key Words : SOFC Triple Combined Cycle, Independent Microgrid, Inertia Force, Large-Scale Solar Power Plant

1. Introduction

Because unstable renewable energy has the large fluctuation given to a microgrid, the amount of introduction to a microgrid is restricted greatly. However, because the microgrid with renewable energy of a high rate is expectable in control of safety, environment, and fossil fuel saving, many study on control of power fluctuation of a microgrid has been reported [1-7]. The power fluctuation of the independent microgrid which interconnects the triple combined cycle (SOFC-TCC) of multi-axis type composed from a solid oxide fuel cell (SOFC), a gas turbine (GT), and a steam turbine (ST) and a large-scale photovoltaic power plant is investigated by numerical analysis. Although the result of research of some SOFC-TCC has been reported until now [8-10], the example of investigation of control of the power fluctuations by interconnection of renewable energy and SOFC-TCC is not found. Generally, the electricity change for several minutes or less is described as cyclic fluctuation, and the electricity change from several minutes to about 20 minutes is described as short period fluctuation. Furthermore, the electricity change exceeding 20 minutes is described as sustained fluctuation. Not only cyclic fluctuation but the component

of sustained fluctuation includes fluctuation of renewable energy. Many system designs in consideration of fluctuations of photovoltaics have been reported [11-16]. Cyclic fluctuations by the weather, short period fluctuations and sustained fluctuations by the solar location, and also sustained fluctuations by the difference in seasonally are contained in photovoltaics power supply. Therefore, in this paper, the effect of electricity stabilization by output adjustment of the SOFC-TCC is investigated about the interconnection system of independent microgrid and SOFC-TCC with large-scale photovoltaics. Because the independent microgrid with renewable energy cannot perform absorption of power fluctuations by interconnection with other power networks, stabilization of the electricity of the microgrid is very difficult [17-21]. In order to control the power fluctuations by renewable energy, technology which the difference of the supply-and-demand balance of the microgrid can control at high speed needs to be introduced.

Although stabilization of the electricity by storage-of-electricity equipment is the most common [22-25], equipment cost has a large subject. The toughness of the electricity grid is made to increase in this study by the output adjustment by a governor free control of the SOFC-TCC, and suitable setting of the inertia system of rotary machines (G/T and S/T) [26-29]. When the inertia system of rotary machines is set up appropriately, it will be expected at least that the cyclic fluctuation of electricity can be controlled. Moreover, the governor free control of the rotary machines (GT and ST) is given to fluctuation of electricity short period, and the governor free control of the SOFC is given to the sustained fluctuation. The objective of this study is to set up the inertia system of the rotary machines of a SOFC-TCC appropriately, and also to make the toughness of the electricity grid with large-scale photovoltaics increase by the governor free control of a SOFC, GT, and ST, and is realizing an independent microgrid without a battery

system. Therefore, the difference of the electricity supply and demand of an independent microgrid (found from a frequency deviation) is investigated in modeling the SOFC-TCC and analyzing the response characteristics of the system by MATLAB/Simulink 2013a. From the results of investigation described in the top, relation between the magnitude of the load fluctuation added to the microgrid, and the operation characteristics of the SOFC-TCC, the characteristics of load following and the magnitude of electricity supply-and-demand difference (frequency deviation) is clarified. As a result, the magnitude of the large-scale photovoltaics which can be introduced into the SOFC-TCC can be predicted now.

2. System Configuration

2.1 SOFC Triple Combined Cycle (SOFC-TCC)

2.1.1 Standard Operation

Figure 1 shows the triple combined cycle (SOFC-TCC) which consists of a solid oxide fuel cells (SOFC), gas turbine (G/T), and steam turbine (S/T) which are investigated in this paper. Although reformed gas of natural gas by an external reformer is supplied to the anode of SOFC, a part of unused gas is discharged from the SOFC. On the other hand, although a high temperature compressed air is supplied to the cathode of the SOFC, this compressed air is emission gas of the G/T. Although a part of oxygen in the compressed air supplied to cathode is consumed by the SOFC, a large quantity of excess air is discharged from the SOFC. The emission of the anode and cathode of the SOFC is supplied to a combustion chamber after mixture, combustion gas of high temperature with high pressure is generated by the reformed gas and oxygen in emission. The combustion gas described in the top heats air supplied to the G/T from

the compressor, the high temperature air discharged from the G/T is supplied to the cathode of the SOFC. The high temperature emission discharged from the combustor is supplied to the exhaust heat boiler, and serves as a heat source of steam used for the ST. Moreover, the output power of the G/T and the S/T can be made to increase independently by supplying natural gas to the combustion chamber directly.

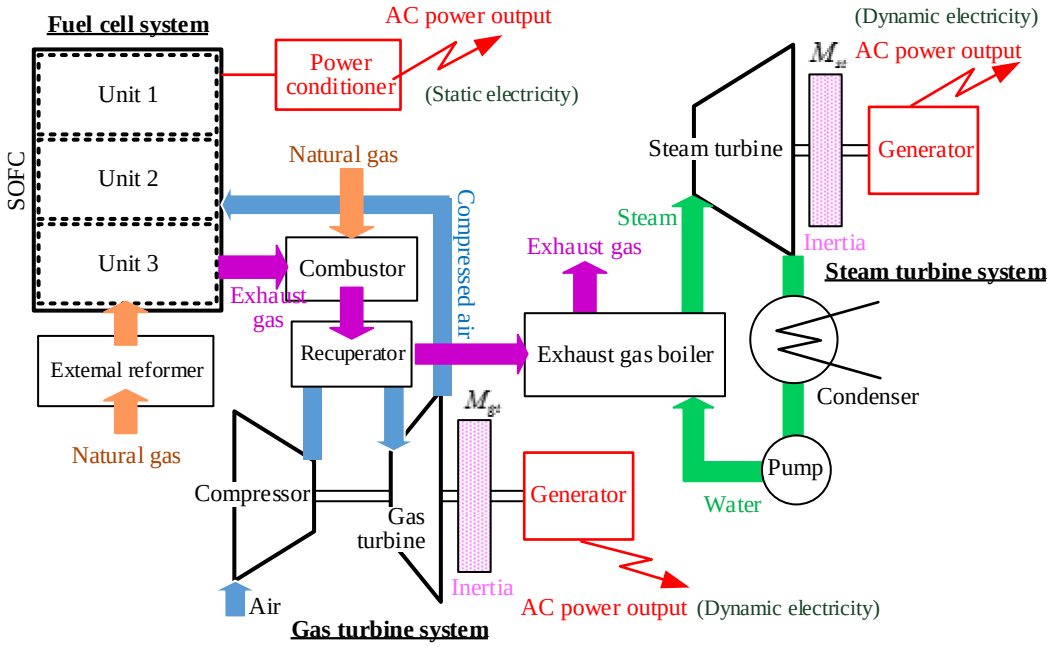

Fig. 1 SOFC triple combined cycle

2.1.2 Dynamic Electricity and Static Electricity

Because the G/T and S/T are rotary machines, they have an inertia force. Therefore, it is thought that the electricity by the G/T and S/T has an effect which controls the power fluctuations concerning the short time of the microgrid (dynamic electricity). Therefore, this paper shows the inertia constants of the G/T and S/T shown in Fig. 1 by M_{gt} and M_{st}, respectively, relation between the values described in the top and the power fluctuations of the

microgrid with a large-scale solar power system is clarified. However, M_{gt} and M_{st} are the inertia constants containing a turbine, power generator, and flywheel of the G/T or the S/T. On the other hand, after the direct current power of the SOFC is converted into AC power by the power conditioner (DC-AC converter and inverter), the AC power is supplied to the microgrid. Because the electricity supplied to the microgrid from the SOFC does not have inertia force, there is almost no control effect of load changes (static electricity). Therefore, it is necessary to show clearly what electricity stabilization is possible by the set values of M_{gt} and M_{st}, and the governor free control of SOFC-TCC on the power fluctuation by renewable energy, and load fluctuation by a demand side.

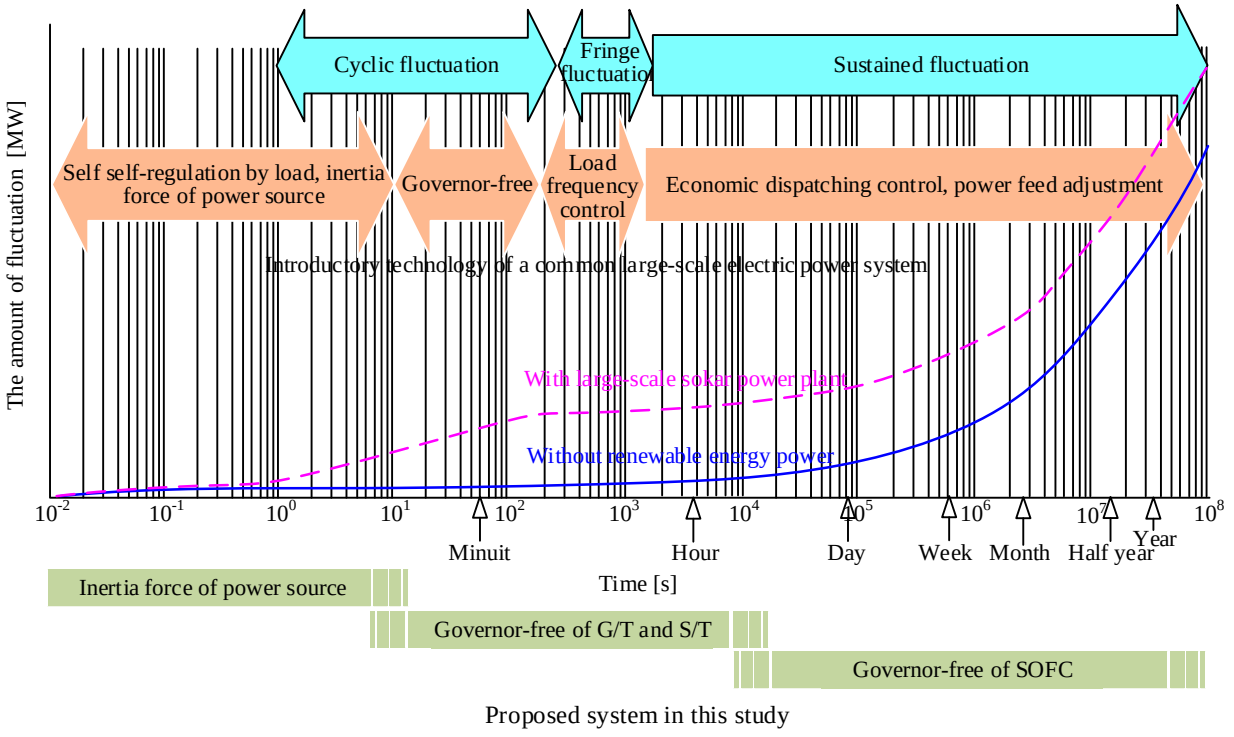

Fig. 2 Electricity fluctuation and control technology

2.2 Dynamic Characteristics of Independent Microgrid

2.2.1 Power Fluctuations and Control Technique

Figure 2 shows the example of the power fluctuations of an independent microgrid. The blue curve in the figure is the relation between the periodic gap of power fluctuation without renewable energy, and the amount of fluctuations. Fluctuations of photovoltaics contains the sudden cyclic fluctuation by the weather, and also fluctuations of the long cycle by daily change or seasonal change (fringe fluctuation and sustained fluctuation) is included. As a result, the amount of fluctuations of electricity increases like the red curve in Fig. 2. In order to stabilize each fluctuation component described in the top, in the common large-scale electric power system, two or more stabilization technique shown in the figure is introduced.

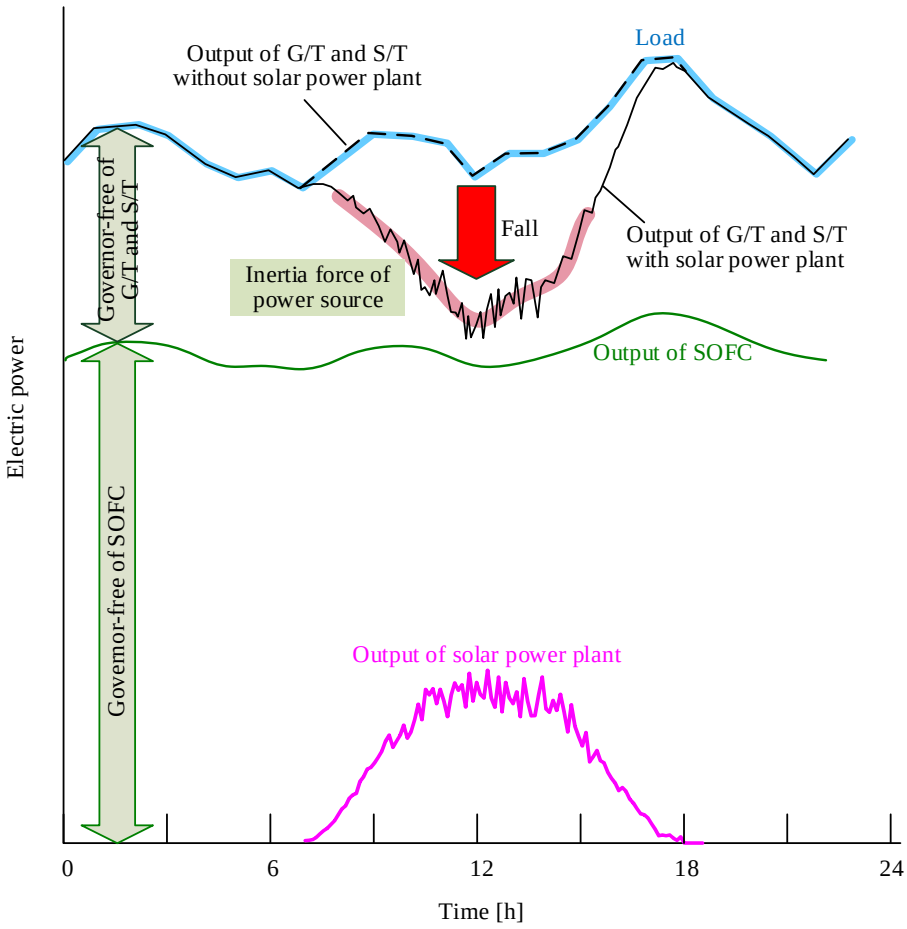

Fig. 3 Operation model of SOFC triple combined cycle with large-scale solar power plant

2.2.2 Power Fluctuations of Proposed System

Figure 3 shows the example of power fluctuation of the proposed system. When there is no output power by photovoltaics, the SOFC-TCC follows the load (blue curve in the figure). On the other hand, the load of the time zone of daytime falls greatly by the output power of photovoltaics (middle under part in Fig. 3) being added to the microgrid. When the load of the microgrid falls rapidly, the output power of the rotary machines (G/T and S/T) of the SOFC-TCC will be adjusted by governor free control, but response time is dependent on the inertia forces of rotary machines. Because the output power of the SOFC is dependent on temperature control, response of the governor free control of the SOFC requires long time compared with rotary machines. Therefore, the power fluctuations of short time of the microgrid is lightened by setting up appropriately inertia constant of GT and ST of the SOFC-TCC, the power fluctuation of furthermore longer time is controlled by the governor free control of the GT. Furthermore, fluctuations of the long period of the microgrid corresponds by the governor free control of the SOFC.

Table 1 Notation for component

i	1	2	3	4	5	6	7
Component	N_2	O_2	H_2	CH_4	H_2O	CO	CO_2

Table 2 Reaction at anode electrode and reformer

Reaction number	Anode reaction	Reaction rate
1	$H_2 + O^{2-} \rightarrow H_2O + 2e^-$	$r_{ad,2}$
2	$CH_4 + H_2O \leftrightarrow CO + 3H_2$	$r_{ad,2}$
3	$CO + H_2O \leftrightarrow CO_2 + H_2$	$r_{ad,3}$
4	$CH_4 + 2H_2O \leftrightarrow CO_2 + 4H_2$	$r_{ad,4}$

Table 3 Reaction at cathode electrode

Reaction number	Cathode reaction	Reaction rate
1	$0.5O_2 + 2e^- \rightarrow O^{2-}$	$r_{cd,1}$

3. Modeling of Equipment

3.1 SOFC

Modeling of mass balance of the SOFC and energy balance is given based on the past report of research [30-33].

3.1.1 Mass balance

Equation (1) is substance balance expression in the anode of the SOFC, i in Eq. (1) is component of the substance shown in Table 1, and $n_{ad,rc}$ is the number of the chemical reactions of the anode and reformer shown in Table 2. On the other hand, Eq. (2) is substance balance expression in the cathode of the SOFC, i in Eq. (2) is a component of the substance shown in Table 1, and $n_{cd,rc}$ is a chemical reaction of the cathode shown in Table 3.

$$\frac{dm_{ad,i}}{dt} = \dot{m}_{ad,in,i} - \dot{m}_{ad,out,i} + \sum_{j=1}^{n_{ad,rc}} a_{ad,ij} r_{ad,j}, \qquad i = 1, ..., 7, \quad n_{ad,rc} = 4 \tag{1}$$

$$\frac{dm_{cd,i}}{dt} = \dot{m}_{cd,in,i} - \dot{m}_{cd,out,i} + \sum_{j=1}^{n_{ad,rc}} a_{cd,ij} r_{cd,j}, \qquad i = 1, ..., 7, \quad n_{cd,rc} = 1 \tag{2}$$

Although an external reformer is introduced in Fig. 1, Mass balance of the external reformer is the same as Eq. (1). $r_{ad,2}$ to $r_{ad,4}$ in Table 2 is a rate of each chemical reaction, and the reaction velocity $r_{ad,1}$ of the anode is obtained by Eq. (3). Moreover, the reaction velocity $r_{ad,2}$ to $r_{ad,4}$ of the reformer is calculated using Eq. (6) from Eq. (4) [31].

$$r_{ad,1} = r_{cd,1} = \frac{I}{2F} \tag{3}$$

$$r_{ad,2} = \frac{k_2}{p_{ad,H_2}^{2.5}} \left(p_{ad,CH_4} p_{ad,H_2O} - \frac{p_{ad,H_2}^3 p_{ad,CO}}{K_2} \right) \Big/ DEN^2 \tag{4}$$

$$r_{ad,3} = \frac{k_3}{p_{ad,H_2}} \left(p_{ad,CO} p_{ad,H_2O} - \frac{p_{ad,H_2} p_{ad,CO_2}}{K_3} \right) \Big/ DEN^2 \tag{5}$$

$$r_{ad,4} = \frac{k_4}{p_{ad,H_2}^{3.5}} \left(p_{ad,CH_4} p_{ad,H_2O}^2 - \frac{p_{ad,H_2}^4 p_{ad,CO_2}}{K_4} \right) \Big/ DEN^2 \tag{6}$$

Here, DEN in Eq. (6) from Eq. (3) is given by Eq. (7), and $K_{ads,i}$ in Eq. (7) is given by Eq. (8). Moreover, rate coefficients for reforming reactions k_2, k_3 and k_4 in Eq. (3) to Eq. (6) are calculated by Eq. (9), the equilibrium constant K_2, K_3 and K_4 of the reaction numbers 2 to 4 in Table 2 is given by Eq. (10) to Eq. (12), respectively.

$$DEN = 1 + K_{ads,CO} p_{ad,CO} + K_{ads,H_2} p_{ad,H_2} + K_{ads,CH_4} p_{ad,CH_4} + K_{ads,H_2O} p_{ad,H_2O} \Big/ p_{H_2} \tag{7}$$

$$K_{ads,i} = A_{K_{ads,i}} \exp\left(\frac{-\Delta \bar{h}_{ads,i}}{RT} \right), \qquad i = H_2,\ CH_4,\ H_2O,\ CO \tag{8}$$

$$k_j = A_{k_j} \exp\left(\frac{-E_j}{R \cdot T} \right), \qquad j = 2,\ 3,\ 4 \tag{9}$$

$$K_2 = \exp\left(-26830/T + 30.114\right) \tag{10}$$

$$K_3 = \exp\left(4400/T - 4.036\right) \tag{11}$$

$$K_4 = \exp\left(-22430/T + 26.078\right) \tag{12}$$

The molar flow rate discharged from the anode and cathode is using choked exhaust flow equation, and when the pressure difference of the inlet port and outlet port of each electrode is

taken into consideration, the molar flow rate is given by the Eqs. (13) and (14) [34]. Moreover, Eq. (15) is a formula of the oxygen utilization factor and fuel (hydrogen) utilization factor of the cathode electrode and the anode electrode.

$$\dot{m}_{ad,out} = \sqrt{k_{ad}\left(p_{ad} - p_{ad,out}\right)} \tag{13}$$

$$\dot{m}_{cd,out} = \sqrt{k_{cd}\left(p_{cd} - p_{cd,out}\right)} \tag{14}$$

$$u_{O_2} = 1 - \frac{\dot{m}_{out,O_2}}{\dot{m}_{in,O_2}}, \qquad u_{H_2} = 1 - \frac{\dot{m}_{out,H_2}}{\dot{m}_{in,H_2}} \tag{15}$$

3.1.2 Energy balance

Equation (16) is an energy balance equation of the whole SOFC [32, 33]. The temperature change of differential time of the SOFC balances the sum total of enthalpy change of the anode and cathode, the energetic change of chemical reactions, DC (direct-current) power output (P_{DC}), and thermal radiation and heat radiation of heat transmission (P_{rad} , P_{ht}). N in Eq. (16) is the number of components of the substance shown in Table 1, and M is the number of the chemical reactions of the anode and the reformer shown in Table 2.

$$C_S \frac{dT}{dt} = \sum_{i=1}^{N} \dot{m}_{ad,in,i}\left(\Delta\bar{h}_{ad,in,i} - \Delta\bar{h}_i\right) + \sum_{i=1}^{N} \dot{m}_{cd,in,i}\left(\Delta\bar{h}_{cd,in,i} - \Delta\bar{h}_i\right) - \sum_{j=1}^{M} \Delta\bar{h}_{rc,j} r_{ad,j} - P_{DC} - P_{rad} - P_{ht} \tag{16}$$

Where, $N = 7$, $M = 4$

Although P_{DC} in an Eq. (16) is obtained by Eq. (17), the stack voltage V of fuel cell is a difference of the open voltage E_{ocv} and voltage loss V_{loss}, as shown in Eq. (18). Moreover, E_{ocv} can be calculated by Eq. (19), and the voltage loss V_{loss} is dependent on the current and temperature of the fuel cell, as shown in Eq. (20) [35].

$$P_{DC} = VI \tag{17}$$

$$V = E_{ocv} - V_{loss} \tag{18}$$

$$E_{ocv} = E_0 + \frac{RT}{2F}\ln\left(\frac{p_{ad,H_2}\, p_{ad,O_2}^{0.5}}{p_{ad,H_2O}}\right) \tag{19}$$

$$V_{loss} = c_1 I + c_2 T + c_3 \tag{20}$$

Equations (21) and (22) are the terms on heat radiation of SOFC in Eq. 16, and take into consideration the thermal radiation P_{rad}, and the heat transmission P_{ht} in this paper.

$$P_{rad} = A\varsigma\sigma\left(T^4 - T_s^4\right), \qquad \sigma = 5.67\times10^{-8}\ W/(m^2\cdot K^4) \tag{21}$$

$$P_{ht} = Ah\left(T - T_s\right) \tag{22}$$

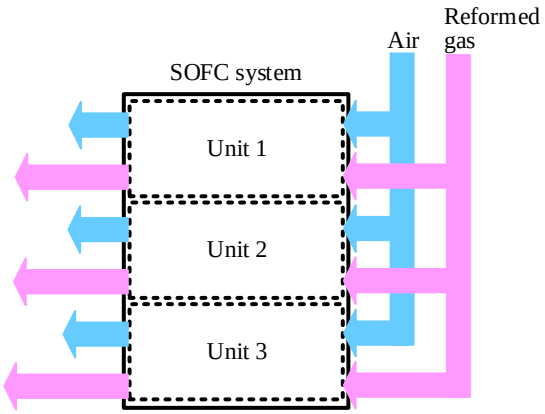

Fig. 4 Parallel connection of SOFC

3.1.3 Stack Unit

Supply of fuel and air to the SOFC assumes the parallel connection of a fuel cell stack, as shown in Fig. 4. In this paper, the number of the fuell cell stacks connected in parallel is described to be the number of units. Because the heat capacity per one unit decreases as this number of units increases and the rated power per unit becomes small, the temperature control by Air flow rate control of SOFC described in Section 4 becomes easy. Therefore, if the number of units of SOFC is made to increase, the following time to load changes will become short. However, because the increase in the number of units leads to the increase in cost of the system, the number of the maximum units in the analysis in this paper is set to 3.

3.1.4 Transfer Function

The transfer function on the output adjustment of SOFC is shown in Eq. (23). T_{fc} in Eq. (23) is a time constant of the output power of SOFC. Because the output power of SOFC is dependent on cell temperature, T_{fc} is decided from the change rate of the cell temperature obtained from the energy balance (Eq. (16)) of the SOFC. s in Eq. (23) is a Laplace operator.

$$P_{fc,out} = \frac{1}{1+T_{fc}s} m_{H_2,in} \tag{23}$$

3.2 Gas Turbine System

3.2.1 Relational Expression of Compressor

The outlet temperature $T_{ac,out}$ in the air compressor of G/T is calculable by Eq. (24) using the outside air temperature T_{amb}. However, change of air in the compressor assumes adiabatic compression, η_{ac}, R_a, $W_{ac,a}$, and γ are compressor efficiency, compression ratio of the compressor, air flow rate of the compressor, and ratio of specific heat of air, respectively.

$$T_{ac,out} = T_{amb}\left\{1+\frac{\left(R_a W_{ac,a}\right)^{\frac{\gamma-1}{\gamma}}-1}{\eta_{ac}}\right\} \tag{24}$$

3.2.2 Gas turbine

Equation (25) is the inlet temperature $T_{gt,in}$ of the gas turbine, and Eq. (26) is the outlet temperature $T_{gt,out}$. Where, the subscript rat shows rating, it is assumed that the flow of combustion gas is the same as the air flow rate from the compressor. Furthermore, W_f in each equation is a fuel flow rate, $W_{ac,a}$ is an air flow rate, and η_t in Eq. (26) is turbine efficiency. Change of the combustion gas in the gas turbine is assumed to be adiabatic expansion.

$$T_{gt,in} = T_{ac,out} + \left(T_{gt,in,rat} - T_{ac,out,rat}\right)\frac{\dot{m}_f}{\dot{m}_{ac,a}} \tag{25}$$

$$T_{gt,out} = \left\{ T_{ac,out} + \left(T_{gt,in,rat} - T_{ac,out,rat} \right) \frac{\dot{m}_f}{\dot{m}_{ac,a}} \right\} \left\{ 1 - \left(1 - \frac{1}{\left(R_a \cdot \dot{m}_{ac,a} \right)^{\frac{\gamma-1}{\gamma}}} \right) \eta_t \right\} \tag{26}$$

3.2.3 Transfer Function

Equation (27) is the transfer function of G/T which used the time constant T_{ac} of the compressor.

$$P_{gt} = \frac{K_{gt} \left\{ \left(T_{gt.in} - T_{gt,out} \right) - \left(T_{ac,out} - T_{outside} \right) \right\} W_a}{1 + T_{ac} s} \tag{27}$$

3.3 Steam turbine

3.3.1 Relational Expression

The model of S/T is Rankine cycle, and as shown in Eq. (32), the external work l_{st} of the S/T is obtained by excluding power consumption l_{pump} of a circulating pump from the quantity of heat P_{boiler} supplied to the exhaust gas boiler. Moreover, $\eta_{th,st}$ in Eq. (32) is theoretical thermal efficiency.

$$l_{st} = P_{boiler} \eta_{th,st} + l_{pump} \tag{32}$$

3.3.2 Transfer Function

Because steam of the exhaust gas boiler is inputted into a turbine after going via steam pipes etc., the output power of the S/T occurs a time-lag (steam-receiver model). Therefore, in this paper, the time constant of the steam receiver is expressed by T_v , and the transfer function is

given by Eq. (33). Moreover, the transfer function of the output power of the S/T is given by Eq. (34) using the delay time constant T_{boiler} of the exhaust-heat-recovery boiler, and the steam-turbine power coefficient K_{st}.

$$P_{out} = \frac{1}{1+T_v s} P_{in} \tag{33}$$

$$P_{st} = \frac{K_{st} T_e W_v}{1+T_{boiler}\, s} \tag{34}$$

3.4 Heat exchange

Equation (35) is a heat balance equation of the heat exchanger. Moreover, the temperature change of heat and cooling of the fluid by a heat exchanger is obtained by Eqs. (36) and (37).

$$P_{he} = K_h A_{he} \Delta T \tag{35}$$

$$\frac{dT_{out,hot}}{dt} = \frac{1}{\tau}\left(T_{in,hot} - T_{out,hot} + \frac{-P_{he}}{\dot{m}_{hot} C_{p,hot}} \right) \tag{36}$$

$$\frac{dT_{out,cold}}{dt} = \frac{1}{\tau}\left(T_{in,cold} - T_{out,cold} + \frac{-P_{he}}{\dot{m}_{cold} C_{p,cold}} \right) \tag{37}$$

3.5 Photovoltaics

Figure 5 shows the example of the test results of the amount of global solar radiation which was distributed in the range of several kilometers and measured simultaneously [36]. The curves of each color in the figure are test results of each 20-set global-solar-radiation meter, the red curve is the output power in the case of interconnecting the 20-set measuring instruments.

Maximum-output fluctuation according to the one-set global-solar-radiation meter at the example of Fig. 5 constitutes about 70% of rated power in several seconds. However, when much photovoltaics is made to interconnect, the cyclic fluctuation of the amount of global solar radiation for less than 10 seconds will be controlled to 20% or less of rated power.

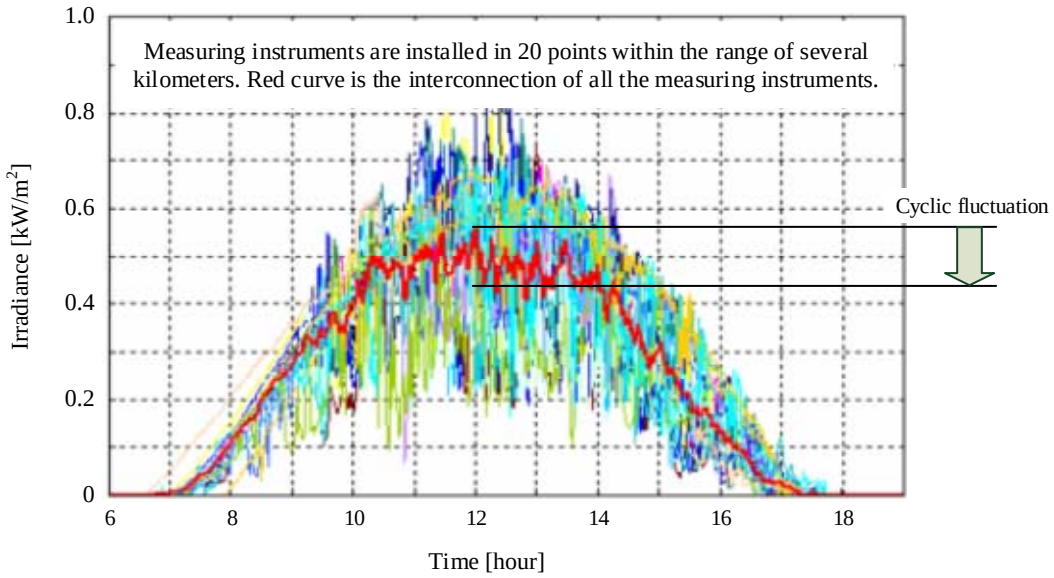

Fig. 5 Experimental results of cyclic fluctuation of global solar radiation

4. System Configuration of SOFC Triple Combined Cycle

4.1 System Configuration and Control Method

Figure 6 is detailed plan of the system configuration of proposal SOFC-TCC. The models of Section 3 is used for material balance, energy balance, and response characteristic (transfer function). Moreover, SOFC consists of three units and the combined cycle by G/T and S/T is a multi-axis type. Furthermore, the inertia constants of the G/T and S/T are M_{gt} and M_{st}, respectively.

Figure 7 is a control block diagram of the whole independent microgrid containing SOFC-TCC, large-scale photovoltaics, and power load. The output power of SOFC is adjusted with the governor free control of reformed gas, and air flow rate control. The compressed air supplied to the G/T by the exhaust heat of SOFC and combustion of the natural gas m_{cb} is heated. Although the output power of SOFC and the exhaust heat of G/T are adjusted with PID control equipment, operation control of S/T by a controller is not introduced.

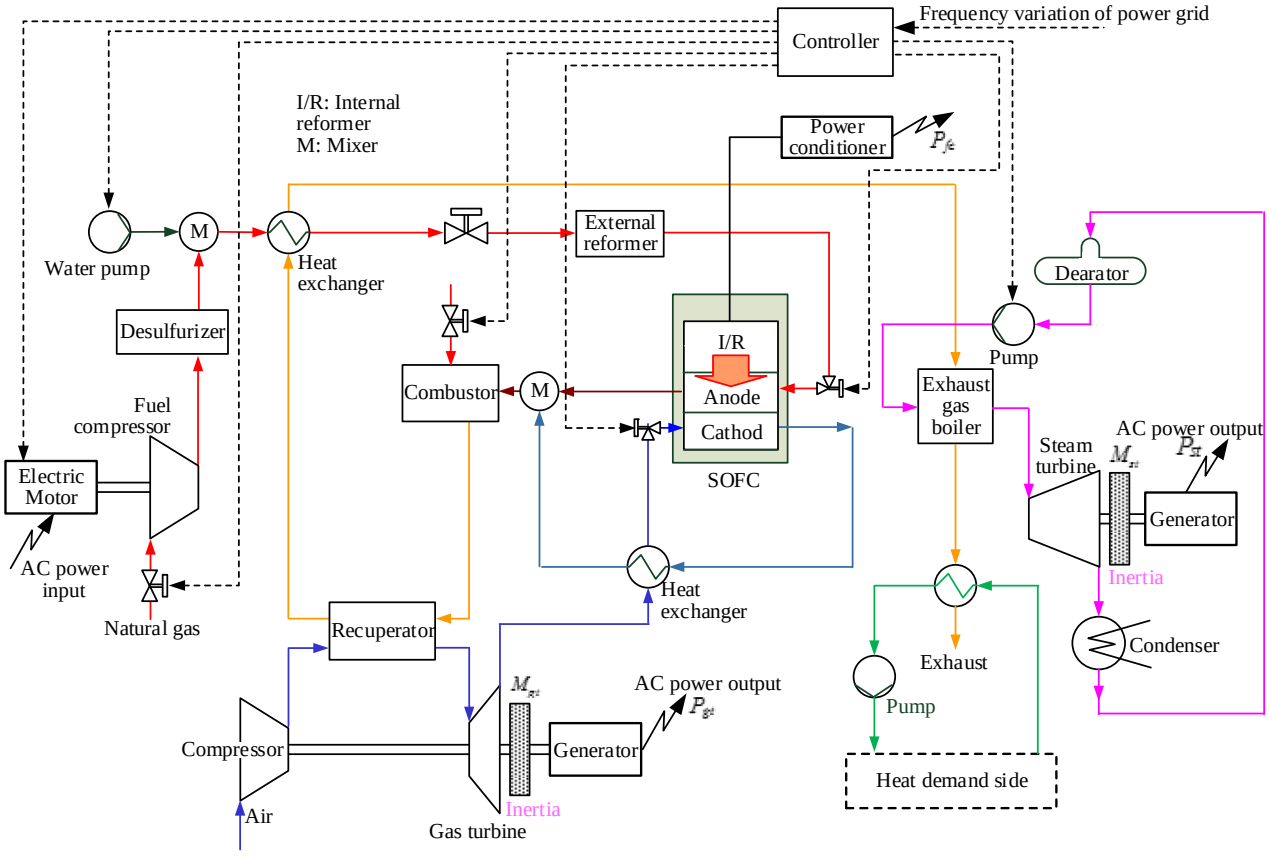

Fig. 6 Block diagram of the SOFC triple combined cycle

4.2 Power Controls and Frequency Changes

The production-of-electricity by the SOFC-TCC and the supply-and-demand difference by power load appear as a frequency deviation of the microgrid, as shown in Eq. (38). Therefore, the production of electricity of the SOFC-TCC can be adjusted by measuring the frequency deviation of the microgrid and giving the PID control equipment in Fig. 7. Figure 8 is a block

diagram of the power controls of proposal SOFC-TCC. Figure 8 (a) shows the power controls of the SOFC-TCC, Fig. 8 (b) is a block diagram in connection with the frequency and effective power of the microgrid [37]. The frequency deviation $\Delta\omega$ of the microgrid is dependent on the difference $(P_g - P_l)$ of the electricity of a power generator and load, and the inertia constant M, as shown in Eq. (38). Equation (39) is a definitional equation of the inertia constant M. The inertia constants M_{gt} and M_{st} of the G/T and S/T are contained in Fig. 8 (b), and the power fluctuation of the short time by the G/T and S/T is controlled by changing these values.

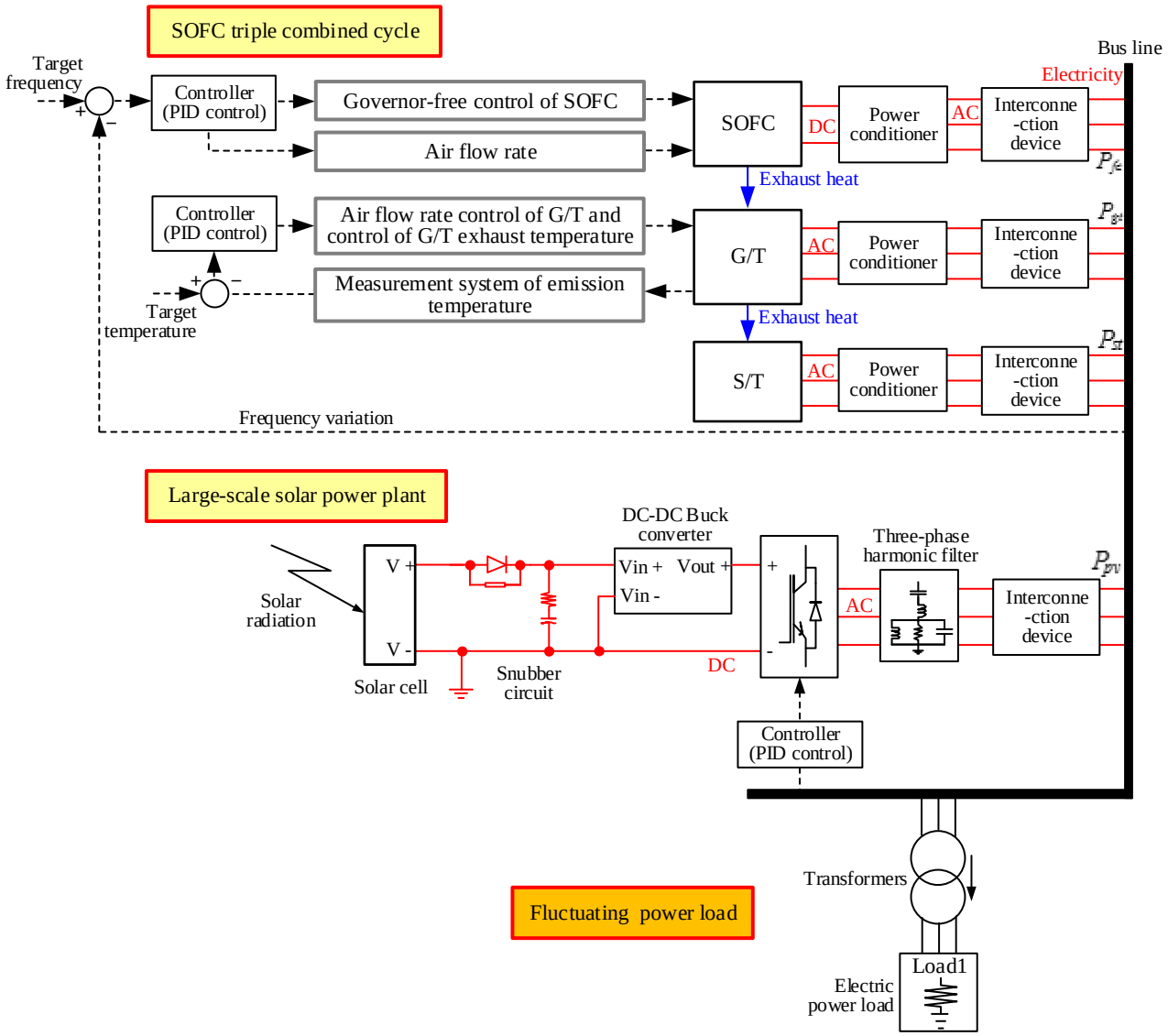

Fig. 7 Whole block diagram of proposed microgrid

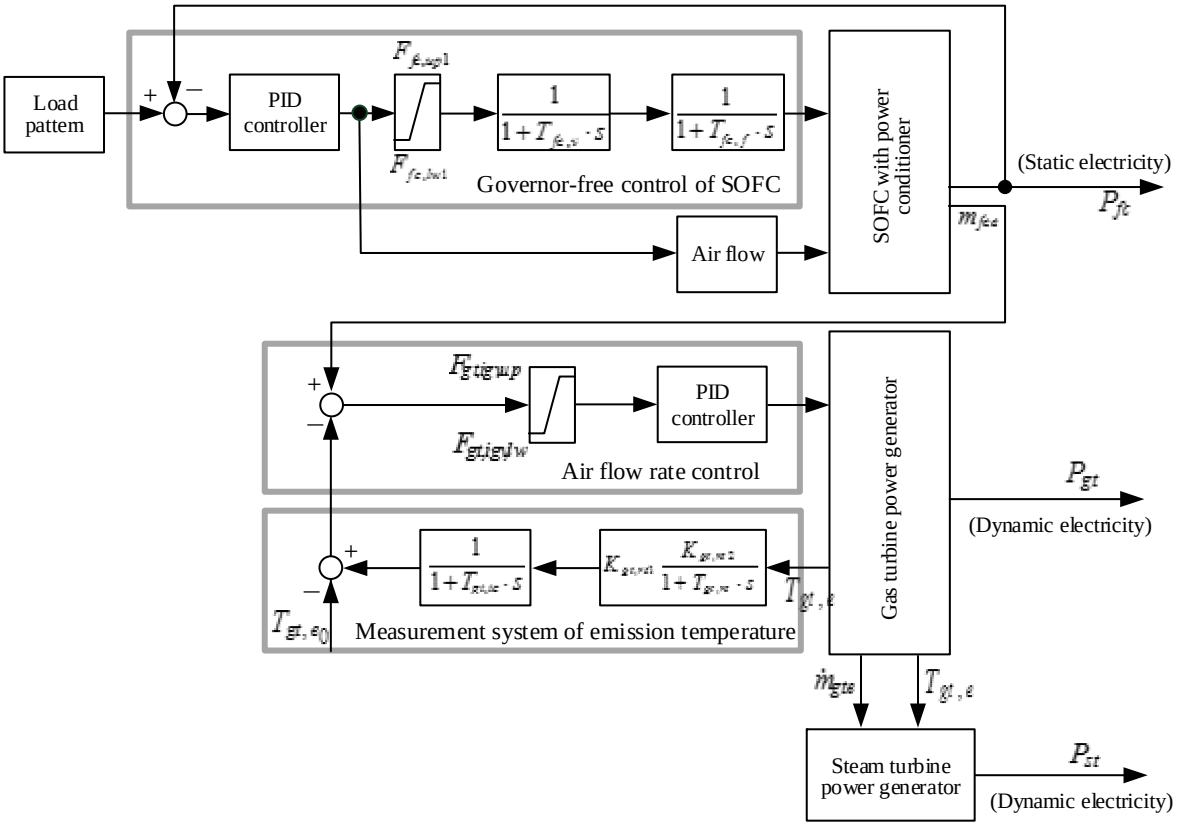

(a) Power output model of each power generator

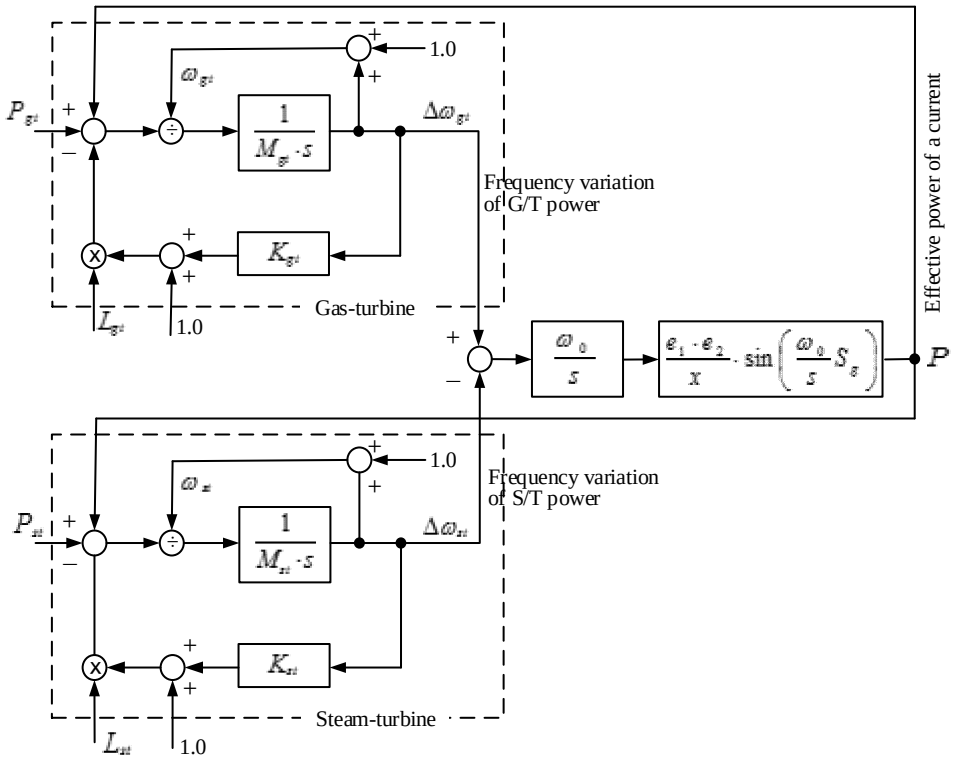

(b) Variability model of system frequency

Fig. 8 Control block diagram of SOFC triple combined cycle

$$\Delta\omega = \frac{1}{Ms}\frac{1}{\omega}\left(P_g - P_l\right) \tag{38}$$

$$M = J\omega = \frac{1}{2}a_r^2 m_r \tag{39}$$

5. Analysis Conditions

5.1 Equipment Specifications and Time Constant

Table 4 is the specifications of the important equipment of the SOFC-TCC assumed in analysis in this paper [38 and 39]. The total production-of-electricity efficiency of the SOFC-TCC at the time of rated operation is 65%, and the production-of-electricity efficiencies of the SOFC, G/T and S/T based on the calorific value of the natural gas of the reformer inlet are 26%, 25%, and 14%, respectively. Table 5 is time constants etc. of the transfer function of important equipment shown in Fig. 8 [40-42]. p.u. in Table 5 is a notation by per-unit system.

5.2 Parameters of PID Control Equipment

The output power of the SOFC model is adjusted by PID control of the governor and air flow showed in Figs. 7 and 8. Equation (40) is the relation between each parameter of PID control equipment, and the output power, and shows the values of these parameters used in this analysis in Table 6. Each parameter of Table 6 decided to converge a transient overshoot in shortest time as less than 3%. Matlab/Simulink 2013a is used for the analysis of the system.

$$U(s) = K_P + K_I\frac{1}{s} + K_D\frac{F_{cl}}{1 + F_{cl}\dfrac{1}{s}} \tag{40}$$

Table 4 Rated state of each equipment

System rated power	1.4 MW
Rated power of SOFC	542 kW
Rated power of G/T	550 kW
Rated power of S/T	308 MW
System frequency	50 Hz
SOFC solid heat capacity	600 J/(kg·K)
Operation conditions	
Anode pressure	0.3 MPa
Cathode pressure	0.3 MPa
SOFC total current	870 A
SOFC cell voltage	0.657 V
SOFC temperature	1113 K
SOFC stack unit power	181 kW
The number of stack unit	3 set
Methane mass flow rate	7.4 g/s
Air mass flow rate	277 g/s
Fuel utilization rate	0.85
Oxygen utilization rate	0.23
Recycle ratio	0.38
Steam/methane ratio	2.0
Outside air temperature t_{amb}	288 K
Compressor outlet temperature $t_{ac,out}$	684 K
G/T entrance temperature $t_{gt,in}$	1573 K
Pressure ratio of compressor R_{ac}	15
Ratio of specific heat γ	1.4
Efficiency of compressor η_{ac}	85 %
Turbine efficiency of G/T η_t	85 %

Table 5 Design parameters and time constants

Equipment		**Governor-free control of G/T**		**Emission temperature control of G/T**	
Power coefficient of gas turbine K_{gt}	0.0021	Fuel upper limit $F_{gt,up2}$	1.0 p.u.	Radiation shield coefficient $K_{gt,rs1}$	0.8
Steam-turbine power coefficient K_{st}	0.000391	Fuel lower limit $F_{gt,lw2}$	0.0 p.u.	Radiation shield coefficient $K_{gt,rs2}$	0.2
Delay time constant of compressor T_{ac}	0.2 s	Possible range of fuel regulation $K_{gt,f}$	0.77	Time constant of radiation shield $T_{gt,rs}$	15 s
Delay time constant of exhaust gas boiler T_b	300 s	Fuel flow rate at the time of no-load $K_{gt,f0}$	0.23	Time constant of thermostat $T_{gt,tg}$	2.5 s
Governor-free control of SOFC		Time constant of flow control valve $T_{gt,v}$	1.0 s	Integral control gain $T_{gt,ic}$	3.3
Fuel upper limit $F_{fc,up1}$	1.0 p.u.	Fuel system time constant $T_{gt,f}$	0.4 s	Time constant of integral control $T_{gt,i}$	250 s
Fuel lower limit $F_{fc,lw2}$	0.0 p.u.	**Air flow rate control of G/T**		Control-signal upper limit of temperature of exhaust gas $F_{gt,up3}$	1.05
Time constant of flow control valve $T_{fc,v}$	1.0 p.u.	Temperature setting bias $B_{gt,tp}$	5 K	Control-signal lower limit of temperature of exhaust gas $F_{gt,lw3}$	0.0
Fuel system time constant $T_{fc,f}$	0.4 p.u.	Integration time constant $T_{gt,itgv}$	773 s	Reference temperature of exhaust gas $t_{gt,ex0}$	858 K
Load and speed control of G/T		Open speed upper limit of air flow rate valve (AFV) $F_{gt,dafv,up}$	0.01 p.u./s		
Speed-regulation gain $K_{gt,sp}$	25	Closed speed upper limit of AFV $F_{gt,dafv,lw}$	-0.01 p.u./s		
Time constant of governor $K_{gt,f}$	0.05 s	Opening upper limit of AFV $F_{gt,up4}$	1.0 p.u.		
Load high limit setting $F_{gt,up1}$	1.05p.u.	Opening lower limit of AFV $F_{gt,lw4}$	0.72 p.u.		
Load low limit setting $F_{gt,lw1}$	-0.1 p.u.				

Table 6 Parameters of PID controller

Number of SOFC	K_P	K_I	K_D	F_{cl}
1 set	0.0001157,	$1.010X10^{-10}$,	1.689,	0.0001740
2 set	0.000673,	$4.565X10^{-9}$,	1.694,	0.0008674
3 set	0.001442,	$1.575X10^{-8}$,	2.300,	0.002186

6. Dynamic-Characteristics Analysis of SOFC

Figure 9 shows the output characteristics of a cold start of the SOFC system which combined the cell stack of SOFC and the reformer. The vertical axis of the figure is expressed by per-unit system based on the rated power (542 kW) of the SOFC. When the fuel cell stack is connected in parallel, the convergence time to rated power will be shortened. Moreover, Fig. 10 shows the analysis results of the number of units and response characteristics when the step load pattern of Fig. 10 (a) is given to the SOFC system. When the number of SOFC units is one, because the time-lag of the temperature control of the SOFC is large, it is difficult to follow the step load of Fig. 10 (a). Moreover, because the time-lag has occurred between the step load and the response even when the number of SOFC units is two, the number of units of SOFC is set as 3 in the following analysis.

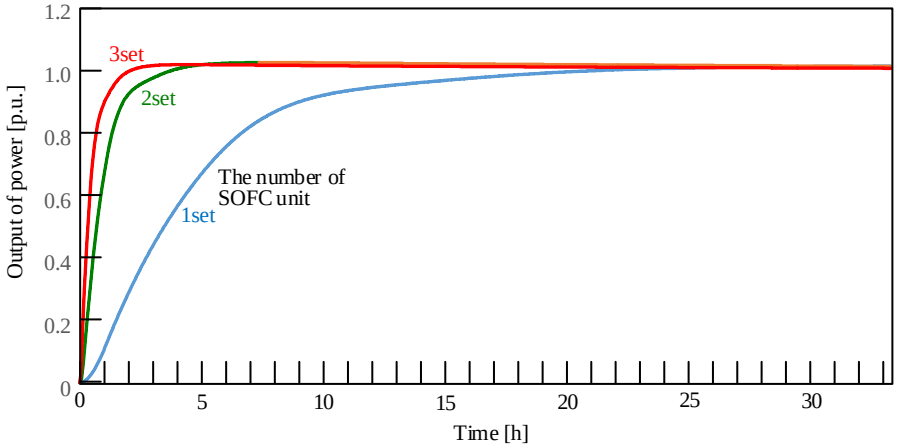

Fig. 9 Dynamic characteristics of SOFC system

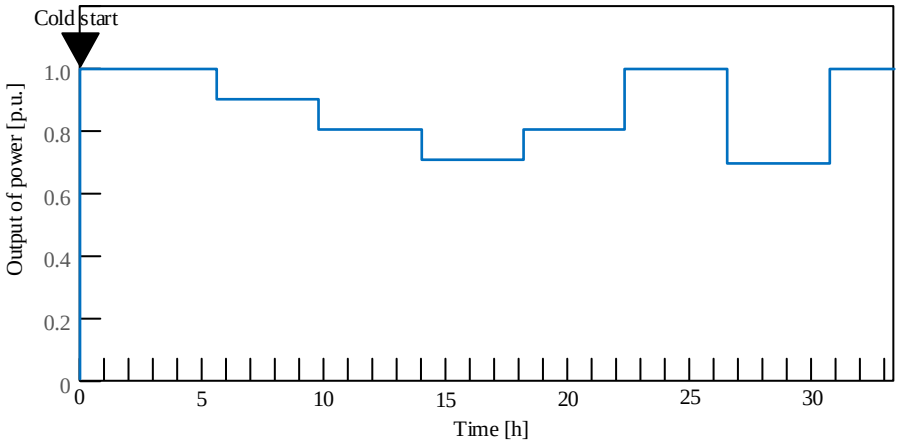

(a) Load pattern

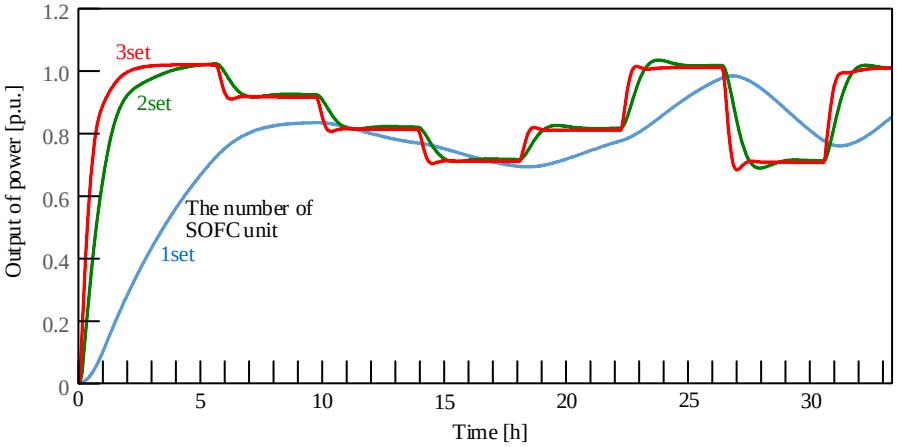

(b) Response of SOFC system

Fig. 10 Dynamic characteristics of SOFC triple combined cycle

7. Dynamic Characteristics of SOFC Triple Combined Cycle (SOFC-TCC)

7.1 SOFC, G/T, Load Distribution of S/T

Figure 11 shows the output characteristics of cold start of the SOFC-TCC in M_{gt}=15 and M_{st}=10. The per-unit system based on 1.4 MW of rated power of the SOFC-TCC is used for Fig. 11. The rates of the rated power of each power generator are SOFC=0.4, G/T=0.38, and S/T=0.22. Because the temperature rise of the cell stack takes long period, obtaining the rated power of the SOFC takes long period. Moreover, speed of response of the S/T is slow by the steam-receiver model as described in Section 3.3.2. As shown in Fig. 11, the settling timeof SOFC and S/T (about

1.8 to 2 hours) is long compared with the G/T operation. Therefore, about power fluctuations of the electricity demand and the photovoltaics for less than 2 hours, the following operation by the G/T becomes important, and the output adjustment of the SOFC and S/T is effective in the power fluctuation in the long periods between one day or seasonally etc.

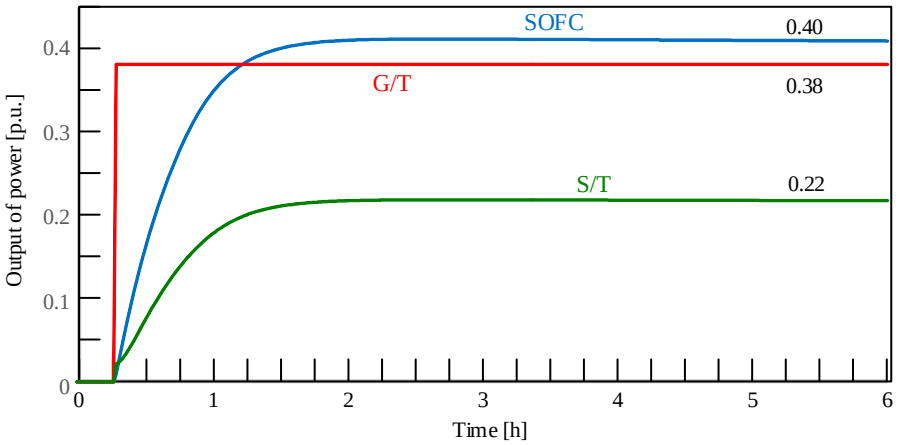

Fig. 11 Output ratio of SOFC triple combined cycle

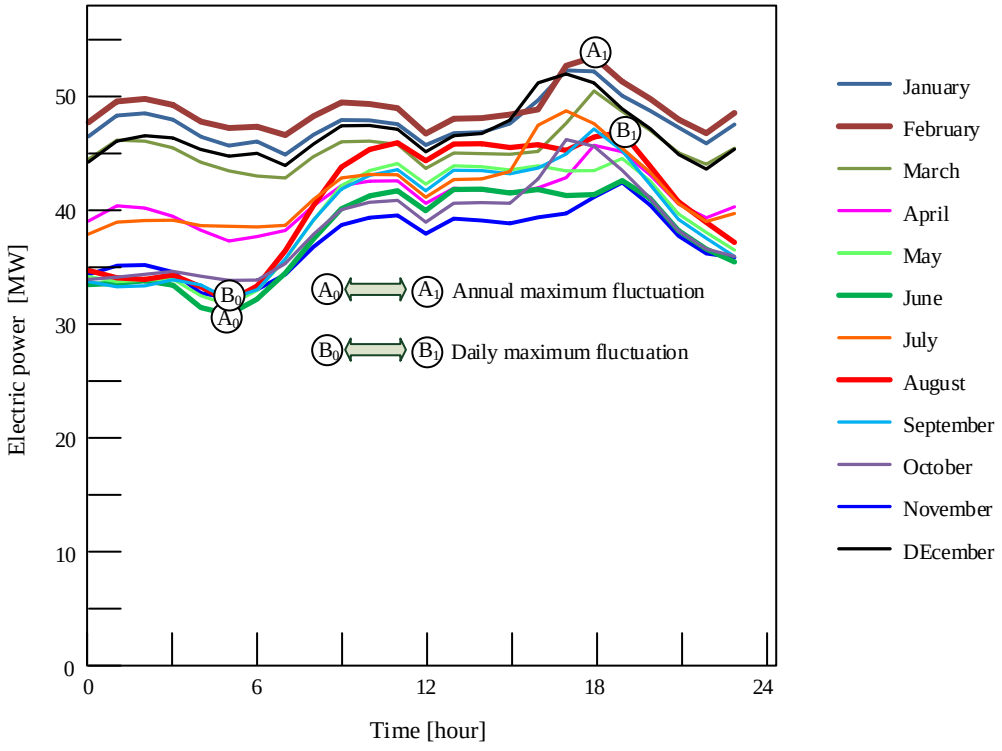

Fig. 12 Electric power demand pattern

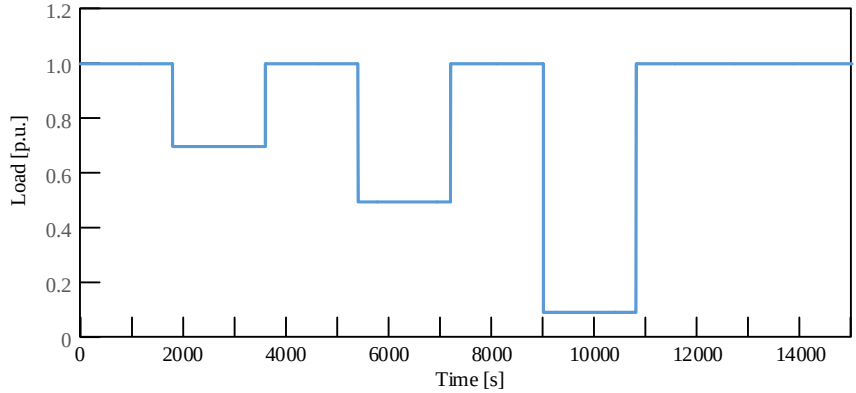

(a) Load pattern

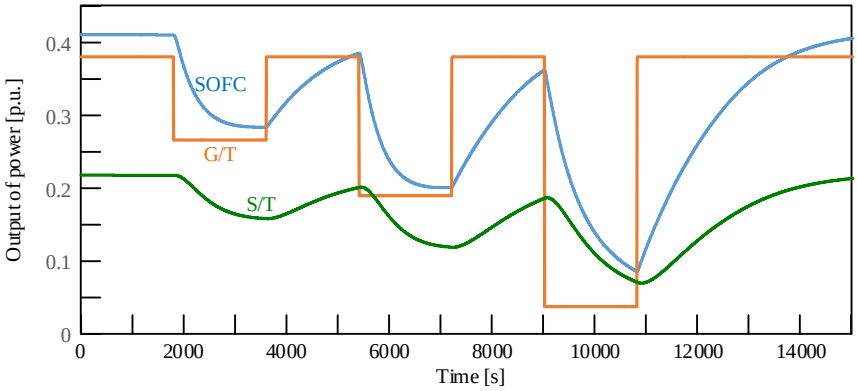

(b) Output from each generator (M_{gt}=15, M_{st}=10)

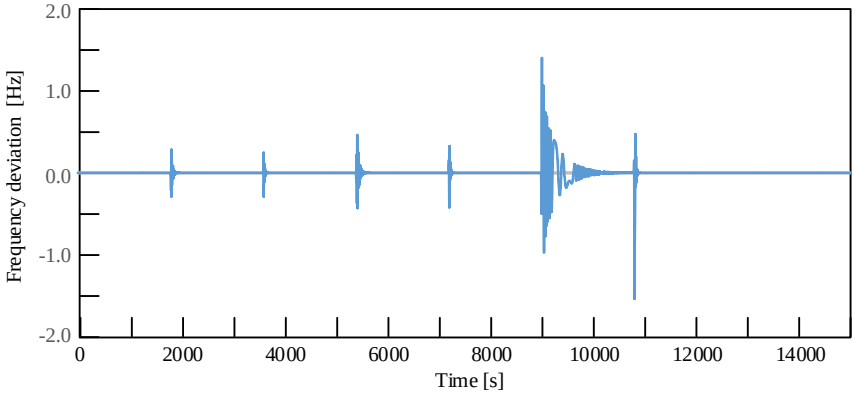

(c) M_{gt}=15, M_{st}=10

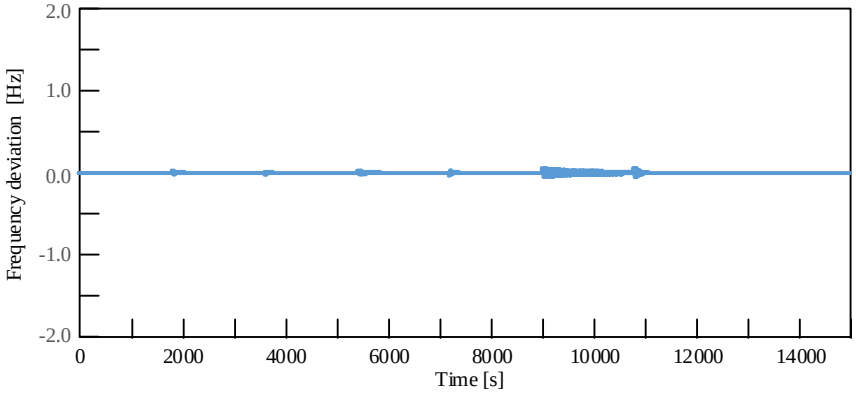

(d) M_{gt}=75, M_{st}=50

Fig. 13 Dynamic characteristics of SOFC triple combined cycle

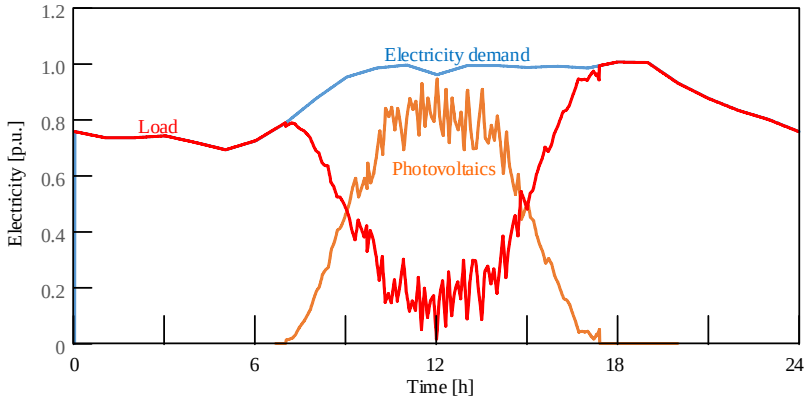

(a) Load pattern

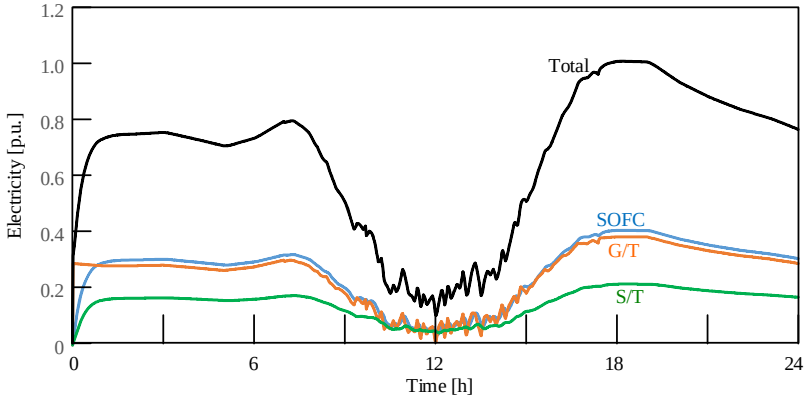

(b) Output from each generator (M_{gt}=15, M_{st}=10)

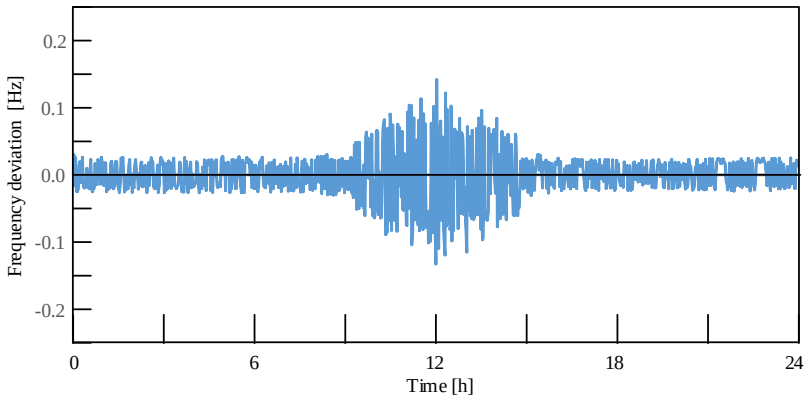

(c) M_{gt}=15, M_{st}=10

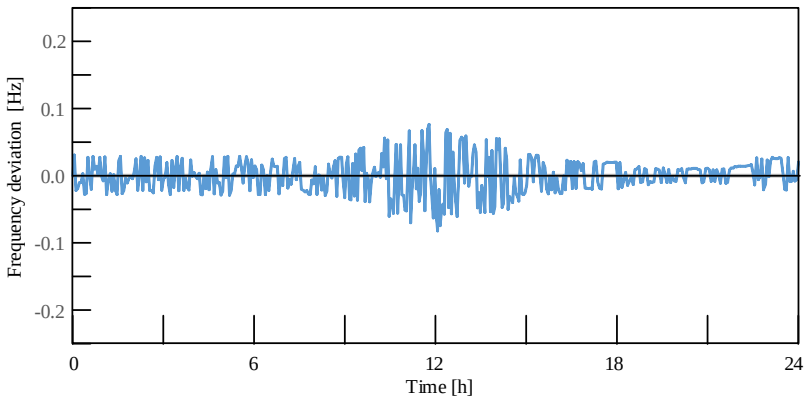

(d) M_{gt}=75, M_{st}=50

Fig. 14 Dynamic characteristics of SOFC triple combined cycle with large-scale photovoltaics

7.2 Load Response Characteristics

Figure 12 shows the power supply pattern in the every month representative day of the Hokkaido Electric Power [43]. Fluctuations of the power load of one day is the largest on August representative days, there is about 40% of difference in day and night. Moreover, fluctuations of the power load for one year is the largest during 5:00 of June representative days, and 18:00 of February representative days, and there is about 44% of difference. Therefore, the step load shown in Fig. 13 (a) is given to the SOFC-TCC from the magnitude of the load fluctuation of Fig. 12. The output characteristics (Fig. 13 (b)) and the frequency deviation (Figs. 13 (c) and (d)) of each power generator at this time were obtained in analysis. Where, Figs. 13 (a) and (b) shows with the per-unit system based on 1.4 MW of rated power of the SOFC-TCC. Because the speed of response of the SOFC and S/T is very slow, when step load is added to the system, reduction of the power variation of 2 hours or less mainly corresponds by the response of the G/T operation as shown in Fig. 13 (b). On the other hand, as shown in Figs. 13 (c) and (d), the characteristics of the frequency deviation about 600 s (10 minutes) of sampling time 9000 s to 9600 s change greatly with setting of the inertia constants M_{gt} and M_{st} of the G/T and S/T, inertia constants have large influence on the cyclic fluctuation and fringe fluctuation (Fig. 2) of the microgrid. Although the ranges of the inertia constant of common G/T and S/T are 10 s to 15 s, because the acceptable value of the frequency deviation in Japan is ±0.2 Hz, the value of M_{gt} and M_{st} in Fig. 13 (c) is not suitable for the microgrid with the large step fluctuation shown in Fig. 13 (a). Moreover, in the results of M_{gt} and M_{st} shown in Fig. 13 (d), frequency deviations serve as value smaller than ±0.2 Hz. Therefore, when fluctuations of the large step load shown in Fig. 13 (a) is expected by the microgrid, it is necessary to set up M_{gt} and M_{st} largely. As described

in the top, the characteristics from cyclic fluctuations (electricity change for several minutes or less) to fringe fluctuations (electricity change for 20 minutes or less) can be adjusted with setting of the inertia constant of the G/T and S/T. Therefore, it is necessary to take into consideration the governor free control of the G/T, and the suitable setting of the inertia force of the G/T and S/T about the cyclic fluctuation and fringe fluctuation, and the sustained fluctuation of 2 hours or less.

7.3 Load Response Characteristics with Photovoltaics

Figure 14 shows the analysis results of output characteristics (Fig. 14 (b)) of each power generator and frequency deviation (Figs. 14 (c) and (d)) by interconnection of the microgrid with large-scale photovoltaics, and the SOFC-TCC. The maximum output of the assumed photovoltaics is the same value as the full power (1.4 MW) of the SOFC-TCC. Therefore, Fig. 14 shows the extreme case where the greatest load change theoretically permitted by the SOFC-TCC is added. Moreover, Figs. 14 (a) and (b) show with the per-unit system based on 1.4 MW of rated power of the SOFC-TCC.

Electricity is supplied to the microgrid with the electricity demand pattern of August representative day with largest daily fluctuation shown in Fig. 12 fromthe 1.4 MW distributed solar cell (accordingly, average amount of insolation in Fig. 5 (red curve)) which enlarged capacity of Fig. 5 and the SOFC-TCC. The load of the SOFC-TCC is red curve excluding the output power of photovoltaics (orange curve) from the electricity demand pattern (blue curve) in Fig. 14 (a). Figures 14 (b) and (c) shows the analysis results in M_{gt}=15 and M_{st}=10. Figure 14 (b) shows the resulst of the output characteristics of each power generator, and Fig. 14 (c)

shows the results of the frequency deviation of the microgrid. As shown in Fig. 14 (c), the frequency deviation is about ±0.14 Hz at the maximum. On the other hand, Fig. 14 (d) shows about ±0.07 Hz at the maximum in the results of the frequency deviation in M_{gt}=75 and M_{st} =50. From the results of Figs. 14 (c) and (d), when large-scale photovoltaics is interconnected to the microgrid, it turns out that fluctuation of a long period to exceed 20 minutes depending on the values of the inertia force of the G/T and S/T also influences.

By the same system as Fig. 14, the relation between the inertia constant of the rotary machines and frequency deviation is shown in Fig. 15. The lower axis (rate of introductory capacity of large-scale photovoltaics) in the figure is a relative rate when the maximum of the output power of the photovoltaics shown in Fig. 14 (a) is set as 1.0. Although the range of the acceptable value of the frequency deviation is ±0.2 Hz, in the case of M_{gt}=3 and M_{st}=2, it is very severe in Fig. 15. Furthermore, it is in order for the frequency deviation (accordingly, supply-and-demand difference of electricity) of the microgrid to become an acceptable range, it is limited to when the interconnection of the distributed photovoltaics shown in Fig. 5 is possible.

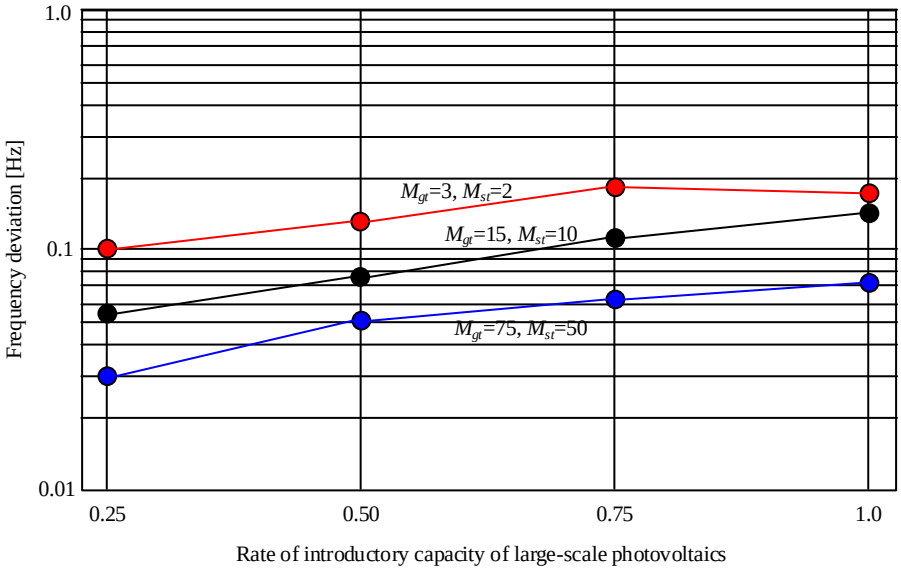

Fig. 15 Relation between the amount of introduction of photovoltaics, and frequency deviation

8. Conclusions

The electricity stabilization at the time of introducing into an independent microgrid with large-scale photovoltaics the triple combined cycle which consists of a solid oxide fuel cell (SOFC, 542 kW), a gas turbine (G/T, 550 kW), and a steam turbine (S/T, 308 kW) was considered. SOFC supplies electricity to the microgrid through an inverter, and the G/T and S/T supply electricity to the microgrid with a synchronous generator. The following conclusions were obtained in this study.

(1) The following to a load changes takes SOFC and S/T about 1.8 to 2 hours. Therefore, the SOFC and S/T can correspond to fluctuations of the electricity demand of the microgrid and photovoltaics output in the long times for one day or seasonally. On the other hand, because the power fluctuation for 2 hours or less is delayed in the response of the SOFC and S/T, It is necessary to make load follow by the governor free control of the G/T.

(2) Setting of the inertia constant of the G/T and S/T showed that the power characteristics of cyclic fluctuation (change for several minutes or less) to fringe fluctuation (change for 20 minutes or less) of the microgrid could be adjusted. Therefore, when the conclusion described in (1) is taken into consideration, in addition to the governor free control of the G/T, it is necessary to set up the inertia constant of the G/T and S/T appropriately about the power fluctuations for 2 hours or less.

(3) Furthermore, when interconnecting larger-scale photovoltaics to the microgrid, the inertia force of the G/T and S/T showed clearly to have influence to the power fluctuations in the long period exceeding 20 minutes.

Nomenclature

A	:	SOFC surface area [m2]
A_i	:	Pre-exponential factor for i
a	:	Stoichiometric matrix
a_r	:	Radius of rotor plate [m]
C_p	:	Specific heat at constant pressure [J/K]
C_S	:	Heat capacity [J/K]
c	:	Constant number
DEN	:	Denominator
E	:	Activity energy [J/mol]
E_{ocv}	:	Open circuit voltage [V]
e_1 , e_2	:	Both-ends voltage of equivalent interconnection line [p.u.]
F	:	Faraday constant (96485 sA /mol)
F_{cl}	:	Filter factor of PID control
h	:	Heat transfer coefficient [W/(m2K)]
$\Delta\bar{h}$	:	Molar specific enthalpy [J/mol]
I	:	Current [A]
J	:	Moment of inertia [kgm2]
K	:	Equilibrium constant
K_{ads}	:	Adsorption constant
K_{gt}	:	Power coefficient of gas turbine
K_h	:	Coefficient of overall heat transfer [W/(m2K)]

K_D, K_I, K_P : Parameter of PID control

K_{st} : Power coefficient of steam turbine

K_{gt} : Power coefficient of gas turbine

k : Rate coefficients for reforming reactions

L : Load [p.u.]

l : External work rate [Nm/s]

M : Factor of inertia

m : Number of moles [mol]

$\dot{m}$: Moles rate [mol/s]

m_r : Mass of rotor plate [kg]

$n_{ad,rc}$: Number of chemical reactions in anode

$n_{cd,rc}$: Number of chemical reactions in cathode

P : Power [W], [p.u.]

p : Pressure [Pa]

R : Universal gas constant [J/(molK)]

R_a : Compression ratio

r : Reaction rate [mol/s]

S_g : Slip [p.u.]

s : Laplace operator

T : Temperature [K]

T_e : Exhaust gas temperature of SOFC [K]

T_i : Delay time constant for equipment i

T_s : Surrounding temperature

ΔT : Difference in temperature [K]

t : Time [s]

u : Utilization

V : Voltage [V]

W : Quantity of flow [p.u.]

Greek characters

γ : Ratio of specific heat

η : Efficiency

ω : Turbine revolving speed

ω_0 : Rated frequency

$\Delta\omega$: Deviation of turbine revolving speed (=frequency deviation)

σ : Stefan-Boltzmann constant (5.67×10-8 J/(sm2K4))

ς : Shaping factor

τ : Time constant

Subscript

ac : Air compressor

amb : Ambiance

DC : Direct current

e : Exhaust

fc : Fuel cell

g : Generation

gt	:	Gas turbine
he	:	Heat exchanger
ht	:	Heat transfer
l	:	Load
lw	:	Lower
rad	:	Heat radiation
st	:	Steam turbine
up	:	Upper
v	:	Vapor

References

[1] Nandar C S A, Robust PI control of smart controllable load for frequency stabilization of microgrid power system. Renewable Energy 2013;56:16-23.

[2] Ngamroo I, Application of electrolyzer to alleviate power fluctuation in a stand alone microgrid based on an optimal fuzzy PID control. International Journal of Electrical Power & Energy Systems 2012;43:969-976.

[3] Nandar C S A, Robust PI control of smart controllable load for frequency stabilization of microgrid power system. Renewable Energy 2013;56:16-23.

[4] Vachirasricirikul S, Ngamroo I, Robust controller design of heat pump and plug-in hybrid electric vehicle for frequency control in a smart microgrid based on specified-structure mixed H2/H∞ control technique. Applied Energy 2011;88:3860-3868.

[5] Jia H, Mu Y, Qi Y, A statistical model to determine the capacity of battery–supercapacitor

hybrid energy storage system in autonomous microgrid. International Journal of Electrical Power & Energy Systems 2014;54:516-524.

[6] Ou T C, Hong C M, Dynamic operation and control of microgrid hybrid power systems. Energy 2014;66:314-323.

[7] Saejia M, Ngamroo I, Stabilization of microgrid with intermittent renewable energy sources by SMES with optimal coil size. Physica C: Superconductivity, 2011;471:1385-1389.

[8] Choi J H, Ahn J H, Kim T S, Performance of a triple power generation cycle combining gas/steam turbine combined cycle and solid oxide fuel cell and the influence of carbon capture. Applied Thermal Engineering 2014;71:301-309.

[9] Arsalis A, Thermoeconomic modeling and parametric study of hybrid SOFC–gas turbine–steam turbine power plants ranging from 1.5 to 10 MWe. Journal of Power Sources 2008;181:313-326.

[10] Mitsubishi to develop SOFC-turbine triple combined cycle system. Fuel Cells Bulletin 2012;7:5-6.

[11] Daud M Z,Mohamed A, Hannan M A, An improved control method of battery energy storage system for hourly dispatch of photovoltaic power sources. Energy Conversion and Management 2013;73:256-270.

[12] Koohi-Kamali S, Rahim N A, Mokhlis H, Smart power management algorithm in microgrid consisting of photovoltaic, diesel, and battery storage plants considering variations in sunlight, temperature, and load. Energy Conversion and Management 2014;84:562-582.

[13] Datta M, Senjyu T, Yona A, Funabashi T, A fuzzy based method for leveling output power fluctuations of photovoltaic-diesel hybrid power system. Renewable Energy 2011;36:1693-1703.

[14] Marcos J, Storkël O, Marroyo , Garcia M, Lorenzo E, Storage requirements for PV power ramp-rate control. Solar Energy 2014;99:28-35.

[15] Wang J, Li X, Yang H, Kong S, Design and Realization of Microgrid Composing of Photovoltaic and Energy Storage System. Energy Procedia 2011;12:1008-1014.

[16] Ou T C, Hong C M, Dynamic operation and control of microgrid hybrid power systems. Energy 2014;66:314-323.

[17] Tao Ma, Hongxing Y, Lin L, Performance evaluation of a stand-alone photovoltaic system on an isolated island in Hong Kong. Applied Energy 2013;112:663-672.

[18] Xiandong M, Yifei W, Jianrong Q, Generic model of a community-based microgrid integrating wind turbines, photovoltaics and CHP generations. Applied Energy 2013;112:1475-1482.

[19] Manoj D, Tomonobu S, Atsushi Y, Toshihisa F, Chul-Hwan K, Photovoltaic output power fluctuations smoothing methods for single and multiple PV generators. Current Applied Physics 2010;10:265-270.

[20] Qi Z, Benjamin C M, Tezuka T, Ishihara K, An integrated model for long-term power generation planning toward future smart electricity systems. Applied Energy 2013;112:1424-1437.

[21] Samir S, Denkenberger D, Williams R, Optimization of specific rating for wind turbine arrays coupled to compressed air energy storage. Applied Energy 2012;96:222-234.

[22] Rodolfo D, Juan M, Lujano R, Bernal-Agustín J, Comparison of different lead–acid battery lifetime prediction models for use in simulation of stand-alone photovoltaic systems. Applied Energy 2014;115:242-253.

[23] Manuel Jesús V, , José Manuel B, José Manuel A, Optimal sizing for UPS systems based on batteries and/or fuel cell. Applied Energy 2013;105:170-181.

[24] Darcovich K, Henquin E R, Kenney B, Davidson I J, Saldanha N, Beausoleil-Morrison I, Higher-capacity lithium ion battery chemistries for improved residential energy storage with micro-cogeneration. Applied Energy 2013;111:853-861.

[25] Yinjiao X, Wei H, Michael P, Kwok Leung T, State of charge estimation of lithium-ion batteries using the open-circuit voltage at various ambient temperatures. Applied Energy 2014;113:106-115.

[26] Giovanni De F, Vincenzo M, Ramteen S, Simulation of an electric transportation system at The Ohio State University. Applied Energy 2014;113:1686-1691.

[27] Amita M, Saroj R, Short term generation scheduling of cascaded hydro electric system using novel self adaptive inertia weight PSO. International Journal of Electrical Power & Energy Systems 2012;34:1-9/

[28] Bignell W, Saffron H, Nguyen T, Humpage W D, Effects of machine inertia constants on system transient stability. Electric Power Systems Research 1999;51:153-165.

[29] Raghavan M R, Jayachandran R, Analysis of the performance characteristics of a two-inertia power transmission system with a plate clutch. Mechanism and Machine Theory 1989;24:499-503.

[30] Kandepu R, Imsland L, Foss B A, Stiller C, Thorud B, Bolland O, Modeling and control of a SOFC-GT-based autonomous power system. Energy 2007;32:406-417.

[31] Xu J, Froment GF, Methane steam reforming, methanation and water-gas shift; I. Intrinsic kinestics. AIChE Journal 1989;35:88-96.

[32] Thomas P, Simulation of industrial processes for control engineers. Wobourn, MA. USA: Butterworth-Heinemann;1999.

[33] Lukas MD, Lee K Y, Ghezel-Ayagh H, An explicit dynamic model for direct reforming carbonate fuel cell stack. IEEE Trans Energy Conver 2001;16(3).

[34] Padulle´s J, Ault G W, McDonald J R, An integrated SOFC plant dynamic model for power

systems simulation. Journal of Power Sources 2000;86;495–500.

[35] Thorud B, Stiller C, Weydahl T, Bolland O, Karoliussen H, Part-load and load change simulation of tubular SOFC systems. Proceedings of fuel cell forum, Lucerne, 28 June 2 July, 2004.

[36] Output fluctuation and alleviation method of PV, The National Institute of Advanced Industrial Science and Technology (AIST) of Japan, Retrieved from https://unit.aist.go.jp/rcpvt/ci/about_pv/output/fluctuation.html ;2014

[37] Taniguchi H, Electric-power-system analysis –Modeling and Simulation–, Ohmsha, 2009. In Japanese.

[38] Stiller C, Thorud B, Bolland O. Safe dynamic operation of a simple SOFC/GT hybrid cycle. Proceedings of ASME Turbo Expo, 2005.

[39] Hafsia A, Bariza Z, Djamel H, Hocine B M, Andreadis G M, Soumia A, SOFC fuel cell heat production: Analysis. Energy Procedia 2011;6:643–650.

[40] IEEE Working Group on Prime Mover and Energy Supply Models for System Dynamic Performance Studies, IEEE PES 94 WM 185-9 PWRS 1994

[41] Task Force C 4-02-25: Modeling of gas turbines and steam turbines in combined cycle power plant, CIGRE Technical Brochure 2003.

[42] Baba K, Kakimoto N, Dynamic Behavior of Combined Cycle Power Plant for Frequency Drop. IEEJ Transactions on Power and Energy 2002;122:392-400. In Japanese.

[43] Electric power supply data in 2010. Hokkaido Electric Power Co..Inc.; 2014. http://www.hepco.co.jp/english/index.html.